Available online at www.sciencedirect.com
ScienceDirect
Cement and Concrete Research 37 (2007) 1233–1240
Cement and Concrete Research

The influence of relative humidity on structural and chemical changes during carbonation of hydraulic lime

A. El-Turki *, R.J. Ball, G.C. Allen

University of Bristol, Interface Analysis Centre, Oldbury House, 121 St Michael's Hill, Bristol, BS2 8BS, United Kingdom

Received 4 January 2006; accepted 22 May 2007

Abstract

Studies monitoring the carbonation of NHL3.5 hydraulic lime are described. Weight-gain measurements, focused ion beam imaging, X-ray diffraction, X-ray photoelectron spectroscopy and Raman spectroscopy were used to monitor changes in structure and composition occurring in lime pastes after exposure to 100% carbon dioxide at relative humidities of 65 and 97%. Lime paste exposed to a relative humidity (R.H.) of 97% indicated a higher carbonation rate compared to paste exposed to 65% R.H. Surface analysis showed that the sample exposed to a relative humidity of 97% was completely carbonated. No calcium hydroxide was detected. A small amount of calcium hydroxide was, however, present at the surface of the sample exposed to 65% R.H. These observations suggest that high humidity results in the formation of a thin layer of crystalline calcium carbonate covering silicate and hydroxide phases. The actual mass increase of the sample also indicated that uncarbonated calcium hydroxide remained beneath the surface.

Keywords: X-ray diffraction; $Ca(OH)_2$; $CaCO_3$; Mortar; Weight gain

1. Introduction

A recent resurgence in the use of lime mortars within the UK building industry has increased the demand for a knowledge and understanding of their properties, with specific attention being paid to the hardening processes. Lime mortars are produced by mixing lime, sand and water, the ratios of which are determined by the final application. Limes can be categorised into two fundamentally different types, hydraulic and non-hydraulic. Non-hydraulic limes consist predominately of calcium hydroxide and are manufactured by calcining pure limestone. These set by carbonation, the rate of which is determined by the environmental conditions, such as carbon dioxide concentration, relative humidity and temperature. The carbonation of calcium hydroxide can be written simply as:

$$Ca(OH)_{2(s)} + CO_{2(g)} \rightarrow CaCO_{3(s)} + H_2O_{(l)} \quad (1)$$

In some cases, lime with limited exposure to carbon dioxide, for instance in the centre of a thick wall, will take many years to carbonate.

In natural hydraulic limes, dicalcium silicate (C_2S) is the major hydraulic phase but the phases C_2AS, C_3S, C_3A and C_4AF were also detected in small amounts [1]. The latter are most commonly formed in the manufacture of cement at much higher temperatures.

A result of the increased setting rate of hydraulic lime mortars is the ability to build structures more rapidly and allowing their use under water. The type of clay calcined, and, thus, the amount of material present which can form these silicates and aluminates, greatly affects the initial strength development. For this reason, a method of classifying different hydraulic limes has been developed. This uses the designation NHL (natural hydraulic lime) followed by a number (2, 3.5 and 5), which represents the hydraulic reactivity of the mortar, 5 being the most hydraulic [2].

The ability to determine the extent of carbonation [3,4] in a lime-based mortar is important in terms of monitoring strength and structural development. In this study, weight-gain measurement has been used to monitor the carbonation of NHL3.5 paste exposed to carbon dioxide at relative humidities of 65 and 97% over a 6-day period.

* Corresponding author. Tel.: +44 117 331 1175; fax: +44 117 925 5646.
E-mail address: A.El-Turki@bristol.ac.uk (A. El-Turki).

0008-8846/$ - see front matter © 2007 Elsevier Ltd. All rights reserved.
doi:10.1016/j.cemconres.2007.05.002

Table 1
Chemical analysis of the NHL3.5

Chemical composition	(% w/w)
SiO_2	10.5
Al_2O_3	3.8
Fe_2O_3	1.5
CaO	60.9
MgO	1.5
K_2O	0.93
Na_2O	0.11
SO_3	1.43
Cl	0.01
Loss in ignition	20.2
Total	100.91
Insoluble residue	0.9
Calcination loss	9.2
Soluble SO_3	0.52
C_2S	25.0
$Ca(OH)_2$	38.1
$CaCO_3$	20.9
$CaSO_4$	0.9
C_4AF	4.5
C_3A	3.8
C_2AS	3.9
Total	98.0
Cementation index	0.51

Following the exposures, X-ray diffraction (XRD), X-ray photoelectron spectroscopy (XPS) and Raman spectroscopy were used to monitor chemical changes attributed to the carbonation process. Focused ion beam (FIB) imaging and sectioning was used to study changes in structure. For comparison, samples of the as-received NHL3.5 lime and freshly prepared paste were also characterised. These are referred to in the text as powder and paste, respectively.

2. Experimental work

2.1. Sample preparation

Lime pastes were produced by mixing natural hydraulic lime NHL3.5, supplied by Hydraulic Limes Ltd, with deionised water. Wet pastes were placed in a small glass dish 10mm in diameter and 6mm deep, holding approximately 0.5g of paste and of suitable size for the microbalance. Lime pastes were allowed to dry in a dessicator for a period of 24h prior to insertion into the microbalance. The results of a chemical analysis of the natural hydraulic lime used in this study, carried out in Castle Cement's laboratories in Clitheroe, using the appropriate British standards, are given in Table 1.

2.2. Weight-gain measurements

Weight-gain measurements were obtained using a 500mg maximum load microbalance system of 0.2μg sensitivity manufactured by CI Electronics of Salisbury, England, with Robol controllers. Weight, temperature and relative humidity measurements were recorded every 100s. Samples were placed on aluminium pans suspended by high purity Nichrome (nickel 80/chromium 20) wire of 125μm diameter. The weight of each sample before exposure was balanced with small metallic tare weights and an electrical offset. The entire microbalance mechanism, including the head, sample and tare weights, was enclosed within Pyrex glass tubes. Exposure gases were bubbled through a humidifier and passed through a chamber where a humidity reading was taken before entering the microbalance apparatus to be passed over the sample. For more detailed information see work by Allen et al. [5,6]. Premier grade carbon dioxide gas was used with a composition of 10ppm O_2, 5ppm CH_4, 2ppm CO and 25ppm N_2. This gas is referred to as 100% CO_2 within the paper.

2.3. X-ray diffraction (XRD)

X-ray diffraction was carried out using a Philips X'Pert Epitaxy X-ray diffractometer and X'Pert software. Samples were exposed to CuKα radiation of wavelength 1.5405Å and operating voltage of 40kV and 40mA over the 2-theta range 25 to 60°. A step size of 0.02° and a dwell time of 0.5s/step were used. In the case of powder samples, a standard holder was used. Exposed samples were carefully removed from their glass dish and then mounted at the correct level within the sample holder, therefore allowing the surface to be analysed.

2.4. X-ray photoelectron spectroscopy (XPS)

This technique detects the transformation of the outermost atomic layers of the materials and is used in this work to monitor the chemical changes that occurred on the surface of lime mortars after reaction with carbon dioxide. An area of approximately 3mm × 4mm was analysed using a Thermo VG Scientific Escascope spectrometer with an AlKα (1486.6eV) X-ray source, operated at 300W (15kV, 20mA). Wide scan survey spectra were obtained between 1000 and 10eV binding energy (BE) with a step size of 1.0eV. Subsequent high-resolution scans over variable BE ranges with 0.1eV steps, usually taking 10–20min to cover the energy range, were recorded for specific elements of interest: C1s; O1s; and Ca2p regions were considered. The operating vacuum during analysis was approximately 5×10^{-9}mbar. All spectra were corrected for charging effects with respect to the adventitious hydrocarbon C1s peak at 284.8eV and quantified using the sensitivity factors included with the VG Eclipse operating software. PISCES version 2000.2 software was used to carry out peak fitting and quantitative analysis [7].

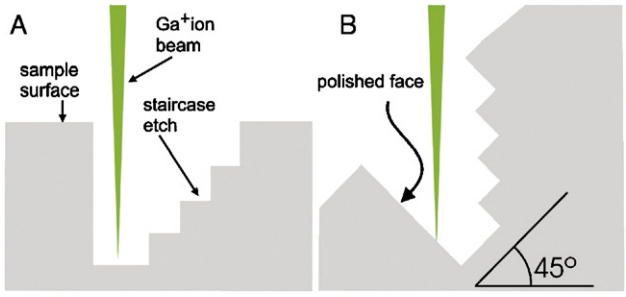

Fig. 1. Illustration of the use of a focused ion beam to mill a hole into the surface of a sample (A) that can be subsequently rotated and imaged (B).

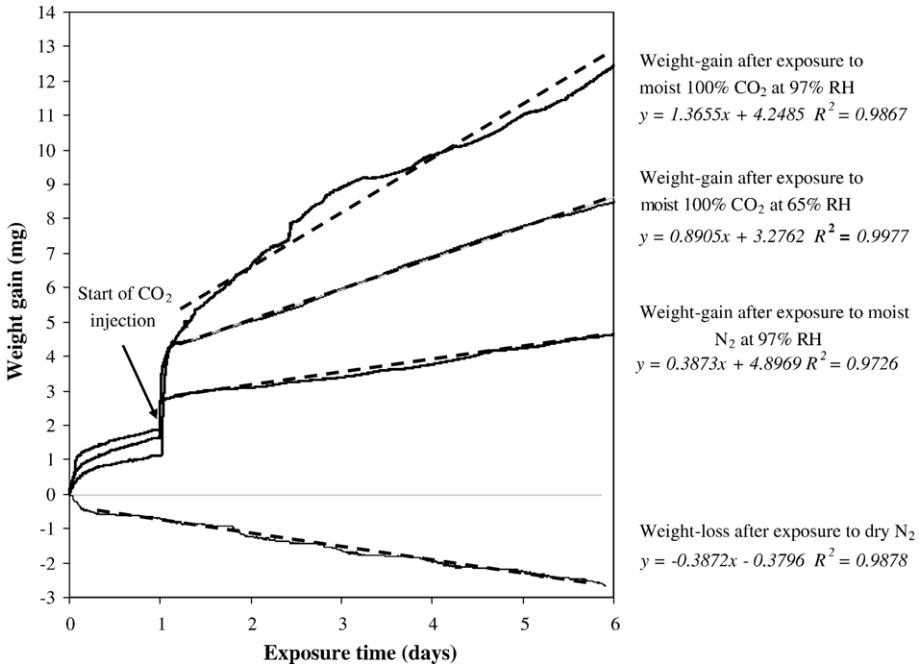

Fig. 2. Weight gain of natural hydraulic lime (NHL3.5) pastes exposed to 100% carbon dioxide at relative humidities of 65 and 97% and N_2 at a relative humidities of 97% and 0% (dry N_2) over a period of 6 days.

2.5. Raman spectroscopy

Sample materials were characterised using a Renishaw Ramascope spectrometer model 2000. The system was equipped with an Ar^+ laser as an excitation source operating at a wavelength of 488nm and maximum laser power of 25mW. The analyses were performed by focusing the laser with objective magnification × 50 onto the sample surface through an Olympus BH2-UMA optical microscope, corresponding to a laser spot diameter of about 4μm. The laser power at the specimen surface was of the order of 3mW and an acquisition time of 10s was used for each spectrum over the wavenumber range 100–4000cm^{-1}. Prior to the analysis, the spectrometer was calibrated using a monocrystalline silicon standard specimen. Peak fitting and deconvolution of Raman spectra were performed using GRAMS32 software.

2.6. Focused ion beam (FIB) imaging

An FEI FIB201 gallium focused ion beam instrument was used for producing high-resolution images at 1pA beam current and up to 300nm beam diameter at 10nA, 30keV. An organometallic gas injector was used for ion-assisted deposition of platinum over selected regions of the sample to avoid electrical charging effects produced under ion bombardment. A higher beam current was then used to mill the sample surface to produce a cross section by firstly depositing a platinum strip across the desired area, acting to protect the structure of the upper sample surface during the etch. A staircase etch was then performed adjacent to the strip, and the edge perpendicular to the surface polished. The sample was then rotated by 45° and the polished cross section imaged, as shown in Fig. 1.

3. Results and discussion

3.1. Weight-gain measurements

Plots of weight gain versus exposure time for two samples exposed to 100% carbon dioxide gas at relative humidities of 65 and 97% are shown in Fig. 2. Samples were exposed to the

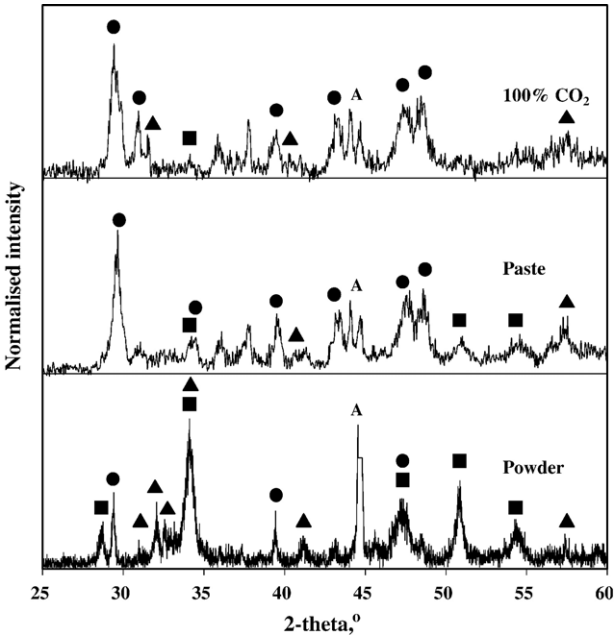

Fig. 3. X-ray diffraction patterns of natural hydraulic lime (NHL3.5) powder, paste and sample exposed to 100% carbon dioxide at a relative humidity of 97% for 5 days. ■ Calcium hydroxide (portlandite), ● calcium carbonate (calcite), ▲ dicalcium silicate (belite), A aluminium peak from sample holder.

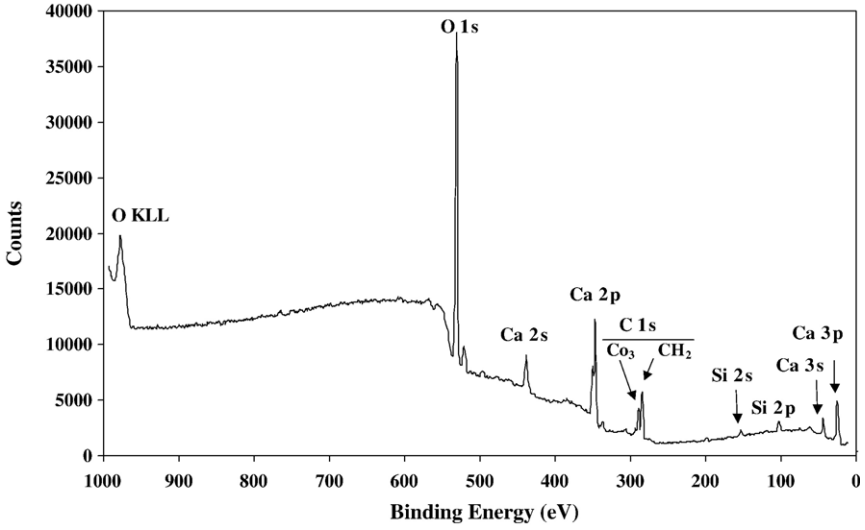

Fig. 4. Wide energy X-ray photoelectron spectroscopy spectrum recorded from hydraulic lime (NHL3.5) paste. Exposure conditions, 100% carbon dioxide at a relative humidity of 97% for 5 days.

humid atmospheres for 5 days but the total period within the balance was 6 days, including an initial 1 day stabilisation period.

The weight gain observed immediately after the injection of humid gas differed for each sample tested. This arose because the samples were dessicated prior to insertion in the microbalance. Hence, exposure to a moist atmosphere showed an immediate weight increase from reabsorption of water vapour prior to equilibrium. This effect did not prejudice the study which was concerned with the steady state weight gain once equilibrium had taken place.

To verify that the initial weight gain was due to water absorption rather than rapid surface carbonation, an experiment was conducted to expose an identical sample of NHL3.5 to 99.995% nitrogen gas (3ppm O_2 and 0.5ppm CH_4 impurities) at relative humidities of 0% (dry) and 97%. The experimental procedure was the same as that described for carbon dioxide and the results are included in Fig. 2. A few hours after the wet nitrogen gas was injected, the rate of weight gain stabilised in a similar way to that observed for the carbon dioxide.

Fitting a least squares law to the sets of data within the time period 1 and 6 days, gave the following equations:

CO_2 at 97% Relative humidity $y = 1.30x + 4.72\ (R^2 = 0.9867)$

CO_2 at 65% Relative humidity $y = 0.89x + 3.28\ (R^2 = 0.9977)$

N_2 at 97% Relative humidity $y = 0.39x + 4.90\ (R^2 = 0.9726)$

N_2 at 0% Relative humidity $y = -0.39x - 0.38\ (R^2 = 0.9726)$

The rate of weight loss of water vapour in dry nitrogen was identical (to within two decimal places) to that of the weight gained in the humid nitrogen atmosphere indicating a process of physisorption rather than chemisorption and that the hydraulic reaction had already taken place on mixing.

Following injection of moist carbon dioxide an initial increase in weight was followed by a steady state weight gain that was linear. The transitional period between the injection of gas and steady state condition was quicker in the sample exposed to 65% relative humidity compared to 97% relative humidity. The rate of weight gain was greater in the 97% relative humidity atmosphere. The combined effect of water absorption and carbonation on weight gain is discussed in Section 4.

3.2. X-ray diffraction (XRD)

X-ray diffraction was used to identify the crystalline phases present in each sample. Peaks were identified in the diffraction patterns relating to calcium hydroxide (portlandite) (JCPDS 87-0674 $Ca(OH)_2$), calcium carbonate (calcite) (86-0174 $CaCO_3$), and dicalcium silicate (belite) (77-0409 Ca_2SiO_4).

The X-ray diffraction patterns obtained are shown in Fig. 3. The pattern corresponding to the natural hydraulic lime (NHL3.5) powder shows the highest proportion of calcium hydroxide (portlandite). The most intense peak on the pattern is located at 34.1° and corresponds to the (011) crystallographic plane in calcium hydroxide. A number of other calcium hydroxide peaks are also shown. Less intense peaks corresponding to calcium carbonate and dicalcium silicate are also present in this pattern and labelled.

The most intense peaks on patterns obtained from the paste and samples exposed to 100% carbon dioxide are located at

Table 2
XPS binding energies

Binding energy (eV)				
C1s	O1s		$Ca2p_{3/2}$	
Carbonate	Carbonate	Hydroxide	Carbonate	Hydroxide
289.61±0.09	530.77±0.02	531.72±0.04	346.65±0.05	347.5±0.2

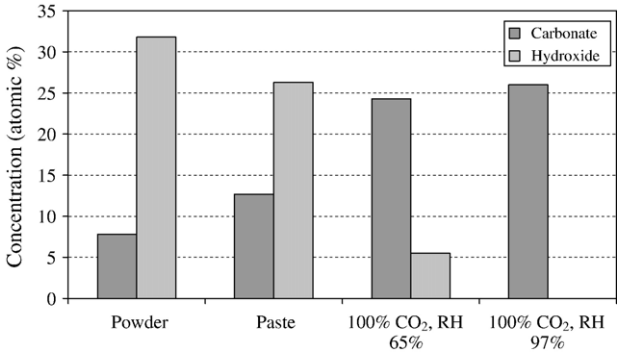

Fig. 5. Concentration of calcium carbonate and hydroxide phases in atomic percent calculated from high-energy resolution XPS data from natural hydraulic lime (NHL3.5) powder, paste and samples exposed to 100% carbon dioxide at relative humilities of 65 and 97% for periods of 6 days.

29.4° and correspond to the (104) crystallographic plane in calcium carbonate. Peaks corresponding to dicalcium silicate are evident in the powder sample, the most intense peak being located at 32.1° and corresponding to the ($\bar{1}$21) crystallographic plane. These peaks are of lower intensity or not visible in the patterns corresponding to the paste and sample exposed to 100% carbon dioxide. This is consistent with the dicalcium silicate reacting with water and becoming coated in a layer of calcium carbonate reducing its ability to be detected. However, the diffraction pattern obtained from the sample exposed to 97% R.H. carbon dioxide revealed that the surface consists of calcium carbonate with a trace amount of calcium hydroxide (Fig. 4) identified by a peak located at 34.1°.

3.3. X-ray photoelectron spectroscopy (XPS)

As received powder, paste and samples exposed to 100% carbon dioxide at relative humidities of 65% and 97% were analysed using XPS. A typical wide scan survey spectrum recorded from the sample exposed to 100% carbon dioxide at a relative humidity of 97% for 5 days is shown in Fig. 4. Peaks are identified on the scan originating from OKLL (Auger), O1s, Ca2s, Ca2p, C1s, Si2s, Si2p, Ca3s and Ca3p interactions. For the purposes of this study, subsequent higher energy resolution scans of specific peaks were conducted on the C1s, O1s and Ca2p regions, as these provide the most relevant information relating to carbonation. Values of binding energy for each peak identified were calculated using PISCES software [7]. The measured binding energies in Table 2 are in agreement with published values in the literature [8,9] specifically the C1s (289.61eV), O1s (530.77eV) and $Ca2p_{3/2}$ (346.65eV) binding energies in high purity powdered calcium carbonate. In addition, the data extracted from the spectra via peak fitting using PISCES software revealed the binding energies of O1s (531.72eV) and $Ca2p_{3/2}$ (347.5eV). These values are in agreement with those recorded in various crystalline calcium silicate hydrates [10].

Intensities of the photoelectron peaks were used to calculate relative concentration in atomic percent for the hydroxide and carbonate phases in each sample examined. These were calculated as the atomic percent of calcium as calcium hydroxide, and calcium as calcium carbonate relative to the total value including all elements detected within the sample. Results are presented in the histogram of Fig. 5. If the ratio in atomic percent between carbonate and hydroxide (8:32) is converted into weight percent a ratio of 1:3 is obtained. This is different from that of the chemical analysis given in Table 1 since the chemical analysis is considering the sample bulk whereas the XPS is a surface technique.

3.4. Raman spectroscopy

Fig. 6 shows Raman spectra recorded from the surface of the freshly prepared lime paste and samples exposed to 100% CO_2 at relative humidities of 65 and 97% respectively. Raman

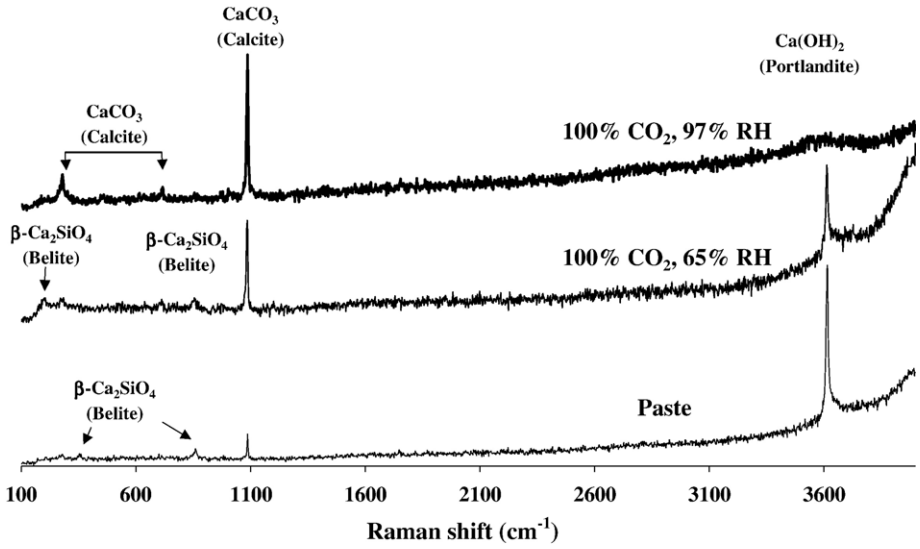

Fig. 6. Raman spectra obtained from natural hydraulic lime (NHL3.5) paste and samples exposed to 100% carbon dioxide at relative humidities of 65 and 97% for 6 days.

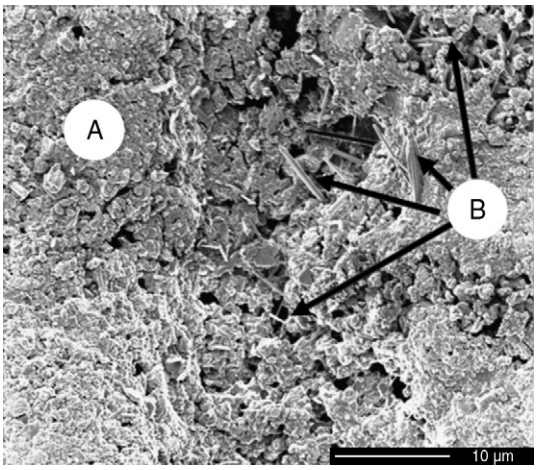

Fig. 7. FIB image of the surface of a freshly prepared natural hydraulic lime paste. A, region of calcium carbonate crystals, B, hydrated silicate crystals.

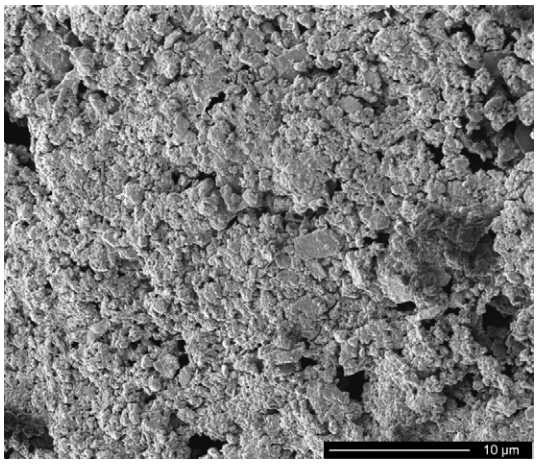

Fig. 9. FIB image of the surface of a natural hydraulic lime paste after exposure to 100% carbon dioxide at a relative humidity of 97%.

spectra recorded from the freshly prepared lime paste sample exhibited a strong band at 3614cm^{-1}. This can be assigned to the main symmetrical stretching vibration mode for the OH^- group in calcium hydroxide, the main component of the lime materials (see Table 1) [11,12]. A small peak located at 1086cm^{-1} is attributed to the main band of the free CO_3^{2-} molecule. This active Raman band can be assigned to the A_{1g} vibrational mode [13,14] and originates from small amounts of calcium carbonate on the surface which probably arose from the reaction of $Ca(OH)_2$ with CO_2 and moisture in the air. Additional peaks located 369cm^{-1} and 858cm^{-1} correspond to β-dicalcium silicate (belite). This phase is contemplated as the major hydraulic phase within the matrix (see Table 1) [1,15].

Examination of the sample exposed to the carbon dioxide at 65% relative humidity indicates variations in the relative proportions of calcium carbonate and calcium hydroxide, in comparison to those of the paste sample. The extent of carbonation of the sample can be determined by considering the relative change in intensity of the strong peaks at 1086cm^{-1} and 3614cm^{-1} relating to calcium carbonate and calcium hydroxide respectively, shown in Fig. 6. Although the peak intensities cannot be compared directly the ratios show a decrease in hydroxide and increase in carbonate. An additional peak located at 253cm^{-1} corresponding to the β-dicalcium silicate (belite) phase from the lime is also observed [15].

Following exposure to carbon dioxide at a relative humidity of 97%, further change is observed in comparison to the spectra discussed previously. The two vibrational modes of the free CO_3^{2-} ion, A_{1g} and E_g at 1085 and 712cm^{-1} respectively, are identified. Of these, the A_{1g} active mode is the strongest by far [13]. There is also a band at 280cm^{-1} which is assigned to an E_g vibration of the crystal lattice, indicative of the complete carbonation at the surface of the corresponding sample [13]. The proportion of $Ca(OH)_2$ compared to $CaCO_3$ becomes very low, with almost total elimination of the OH^- symmetrical stretching at 3614cm^{-1}. In contrast, the sample exposed to a relative humidity of 65% shows a high proportion of calcium hydroxide remaining on the surface (see Fig. 6).

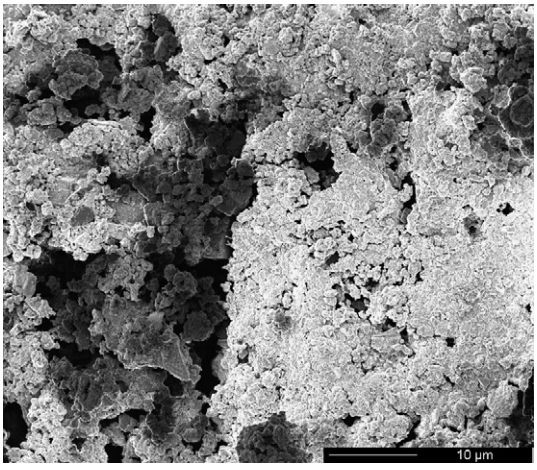

Fig. 8. FIB image of the surface of a natural hydraulic lime paste after exposure to 100% carbon dioxide at a relative humidity of 65%.

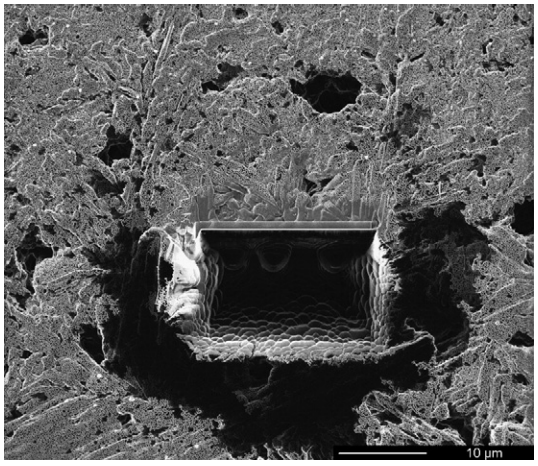

Fig. 10. Focused ion induced image of the surface of a natural hydraulic lime (NHL3.5) lime paste exposed to 100% carbon dioxide at a relative humidity of 97% for 5 days showing calcium carbonate crystals and location of milled hole.

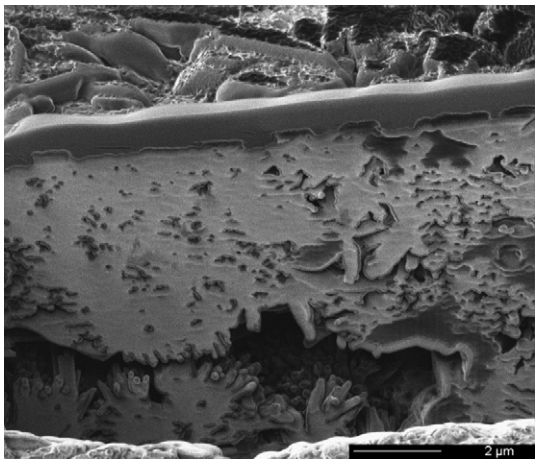

Fig. 11. Focused ion induced image of the polished side of a section milled into the surface of a natural hydraulic lime paste sample after exposure to 100% carbon dioxide at a relative humidity of 97% for 6 days showing underlying calcium carbonate crystals.

3.5. Microstructural analyses

Fig. 7 shows a focused ion beam image taken of the surface of a freshly prepared lime paste. The surface consists predominantly of calcium carbonate (area A) crystals with a morphology resembling that of dicalcium silicate (area B). This is in agreement with the Raman spectra shown in Fig. 6.

Fig. 8 shows a focused ion beam image of the surface of a freshly prepared natural hydraulic lime paste after exposure to 65% relative humidity. The surface comprises of calcium carbonate, calcium silicate crystals are not easily identified at the magnification.

Exposure of the lime paste to an atmosphere of 100% carbon dioxide at a relative humidity of 97% produces a significant change in the morphology, as shown in Fig. 9. It is likely that calcium carbonate crystals have grown to cover the smaller decorative silicate phases.

A focused ion beam instrument was used to mill a cross section of the sample exposed to 100% carbon dioxide at 97% relative humidity, in order to examine the morphology of crystals immediately under the surface. Fig. 10 shows a FIB image of the sample surface and location of the milled section. Fig. 11 shows a higher magnification image of the polished side of the milled hole. A strip of deposited platinum located on the top surface of the specimen during polishing, is seen at the top of the image. A cavity is visible at the bottom of the image, the interior surface of which contains a number of small crystals. These are consistent in form with those of calcium carbonate. However, they are most similar to the aragonite crystal form. This observation is consistent with the work of Martinez-Ramirez et al. [14], who observed the aragonite phase at various depths in a comparable lime mortar sample.

4. General discussion

The analysis of the NHL3.5, given in Table 1, indicates 38.1% calcium hydroxide by weight. The mass of lime in each sample was at least 0.4 g. If total carbonation of all calcium hydroxide contained within the sample is assumed, a minimum increase in weight of 53.5 mg is expected. The highest rate of carbonation observed was 1.3 mg/day in the sample exposed to 97% relative humidity. However, considering that a weight gain of 0.39 mg/day was observed for the sample exposed to N_2 the actual weight gain due to carbonate may be recalculated to 0.97 mg/day and 0.5 mg/day for 97 and 65% R.H. respectively. This suggests that only a small proportion of the calcium hydroxide available to carbonate had actually reacted by the time 5 days of exposure was reached.

High concentrations of carbon dioxide and humidity represent the most favourable conditions for carbonation as these promote the dissolution of carbon dioxide in water to form the CO_3^{2-} ion by the reaction given in Eq. (2).

$$CO_2 + 3H_2O \rightarrow HCO_3^- + H_3O^+ + H_2O \rightarrow CO_3^{2-} + 2H_3O^+. \quad (2)$$

The various analysis techniques used to determine the composition of the sample, namely XRD, XPS and Raman spectroscopy, all indicate that calcium carbonate is the dominant phase with only trace amounts of calcium hydroxide. However, weight-gain results suggest higher amounts of calcium hydroxide within the sample. A probable explanation for this observation is the formation of a calcium carbonate film on the surface of calcium hydroxide particles. This would not only reduce the amount of calcium hydroxide detectable but also reduce the carbonation rate as carbon dioxide would be required to diffuse through this layer.

It is widely accepted that the formation of calcium carbonate on the surface of a lime mortar or paste reduces or blocks pores [16]. A consequence of this would be to reduce the diffusion rate of moisture and carbon dioxide into the sample resulting in the transition observed. The end of the transition zone may indicate that the absorption of water on the internal and external surfaces of the sample has been reached.

5. Conclusions

The microbalance technique has been used to determine the rate of carbonation of a natural hydraulic lime (NHL3.5) paste after exposure to 100% carbon dioxide at relative humidities of 65 and 97%. The following conclusions can be drawn from the results:

1) Carbonation rates of 0.5 and 0.97 mg/day were recorded at relative humidities of 65 and 97% respectively supporting the view that the rate of carbonation rate increases with relative humidity.
2) The rate of carbonation was constant under steady state conditions over 5 days of exposure suggesting a constant rate of carbon dioxide, or carbonic acid.
3) Detailed observations of the underlying microstructure were facilitated using focused ion beam milling.

Acknowledgments

This work was supported by the EPSRC and the DTI Sustainable Technology Initiative Programme.

References

[1] J. Lanas, J.L. Perez Bernal, M.A. Bello, J.I. Alvarez Galindo, Mechanical properties of natural hydraulic lime-based mortars, Cement and Concrete Research 34 (2004) 2191–2201.
[2] G.C. Allen, J. Allen, N. Elton, M. Farey, S. Holmes, P. Livesey, M. Radonjic, Hydraulic lime Mortar for Stone, Brick and Block Masonry, Donhead Publishing Ltd., 2003 ISBN 1 873394 540.
[3] Deuk Ki Lee, An apparent model for the carbonation of calcium oxide by carbon dioxide, Chemical Engineering Journal 100 (2004) 71–77.
[4] K. Van Balen, Carbonation reaction of lime, kinetics at ambient temperature, Cement and Concrete Research 35 (2005) 647–657.
[5] G.C. Allen, A. El-Turki, K.R. Hallam, D. Mclauchlin, M. Stacey, Role of NO_2 and SO_2 in degradation of limestone, British Corrosion Journal 35 (1) (2000) 35–38.
[6] G.C. Allen, A. El-Turki, K.R. Hallam, D. Mclauchlin, M. Stacey, in: D.J. Mitchell, D.E. Searle (Eds.), Role of NO_2 and SO_2 on the Degradation of Limestone in 'Stone Deterioration in Polluted Urban Environments', Science Publishers Inc, Plymouth, UK, 2004, pp. 119–130, Chapter 8.
[7] PISCES (Programmable Interface for Spectrometer Control and Electronics) Version 2000 2, Dayta Systems.
[8] J.F. Moulder, W.F. Stickle, P.E. Sobol, K.D. Bomben, Handbook of X-ray Photoelectron Spectroscopy, Perkin-Elmer Corporation0-9627026-2-5, 1992.
[9] A.B. Christie, J. Lee, I. Sutherland, J.M. Walls, Applied Surface Science 15 (1983) 224–237.
[10] L. Black, K. Garbev, P. Stemmermann, K.R. Hallam, G.C. Allen, X-ray photoelectron study of oxygen bonding in crystalline C–S–H phases, Physics and Chemistry of Minerals 31 (2004) 337–346.
[11] P.H. Baranek, A. Lichanot, R. Orlando, R. Dovesi, Structural and vibrational properties of solid $Mg(OH)_2$ and $Ca(OH)_2$ — performances of various hamiltonians, Chemical Physics Letters 340 (2001) 362–369.
[12] T.Y. Kwon, T. Fujishima, Y. Imai, FT-Raman spectroscopy of calcium hydroxide medicament in root canals, International Endodontic Journal 37 (2004) 489–493.
[13] H.N. Rutt, J.H. Nicola, Raman spectra of carbonates of calcite structure, Journal of Physical Chemistry C: Solid State Physics 7 (1974) 4522–4528.
[14] S. Martinez-Ramirez, S. Sanchez-Cortes, J.V. Garcia-Ramos, C. Domingo, C. Fortes, M.T. Blanco-Varela, Micro-Raman spectroscopy applied to depth profiles of carbonates formed in lime mortar, Cement and Concrete Research 33 (2004) 2063–2068.
[15] R. Corinne, R. Bruno, M. Madon, Raman spectroscopic investigations of dicalcium silicate: polymorphs and high-temperature phase transformations, Journal of the American Ceramic Society 80 (92) (1997) 413–423.
[16] J. Lanas, R. Sirera, J.I. Alvarez, Compositional changes in lime-based mortars exposed to different environments, Thermochimica Acta 429 (2005) 219–226.